Pergamon

Acta mater. Vol. 46, No. 16, pp. 5769–5776, 1998
© 1998 Acta Metallurgica Inc.
Published by Elsevier Science Ltd. All rights reserved
Printed in Great Britain
1359-6454/98 $19.00 + 0.00

PII: S1359-6454(98)00228-6

SLIP BAND PROPAGATION AND SLIP VECTOR TRANSITION IN B2 FeAl SINGLE CRYSTALS

K. YOSHIMI†[1]‡, M. H. YOO[2] and S. HANADA[1]

[1]Institute for Materials Research, Tohoku University, Sendai 980-77, Japan and [2]Metals and Ceramics Division, Oak Ridge National Laboratory, Oak Ridge, TN 37831-6115, U.S.A.

(Received 24 March 1998; accepted 19 June 1998)

Abstract—At the peak temperature, 823 K, of the yield strength anomaly of B2 FeAl, slip band propagation and slip vector transition were investigated using Fe–39 mol% Al single crystals. The single crystal oriented along a compression axis close to the [$\bar{1}$23] direction showed serrated flow during work-hardening at small strains (< 2%). Coarse slip bands propagate in the single crystal specimens, like Lüders band propagation in polycrystals, in the initial strain range. The slip vector was identified by TEM to be parallel to ⟨111⟩ in the early stage of strain corresponding to yielding. Beyond plastic strains of about 3%, serrations disappeared and significant work-softening occurred. The slip vector responsible for the later stage of deformation was observed to be ⟨100⟩. That is, the slip vector changes from ⟨111⟩ to ⟨100⟩ as the plastic strain increases. Because the density of ⟨111⟩ superdislocations is found to be very low after the slip transition, glide decomposition of ⟨111⟩ superdislocations is believed to the primary source mechanism for ⟨100⟩ dislocations. The slip band propagation in B2 single crystals is discussed in comparison with that of other intermetallic single-crystalline materials. © *1998 Acta Metallurgica Inc. Published by Elsevier Science Ltd. All rights reserved.*

1. INTRODUCTION

The slip system at room temperature of B2 FeAl is the same as that of b.c.c. metals and alloys, i.e. on the closed-packed plane, {101}, and along the closed-packed direction, ⟨111⟩. As the test temperature is raised, the slip vector abruptly changes from ⟨111⟩ to ⟨100⟩ at a moderate temperature. This phenomenon is designated as "slip vector transition", which was first revealed by Umakoshi and Yamaguchi [1] in this aluminide. Although the Al composition dependence of the slip vector transition temperature is still under debate, it has been established that this slip vector transition takes place in the entire B2 compositional range [2–5]. In addition, this aluminide exhibits the yield stress anomaly, i.e. a positive temperature dependence of yield stress [3, 6–10]. In our previous work on iron-rich B2 FeAl [3, 11, 12], it has been found that the slip transition is associated with the peak temperature of positive temperature dependence of yield stress. Below the peak temperature of 823 K, the slip vector is ⟨111⟩, and single crystal specimens deform with serrated flow behavior and work-harden monotonously. Above the peak temperature, the slip vector is ⟨100⟩, and single crystal specimens deform without serrations and exhibit large work-softening after yielding (so-called "yield drop"). Around the peak temperature, the appearance of these deformation features depends sensitively on strain and load axis, suggesting that complex and unstable slip vector transition processes occur during deformation.

The purpose of this paper is to investigate slip vector transition of B2 FeAl using a single crystal at the peak temperature. It will be shown that the slip vector changes from the ⟨111⟩ to ⟨100⟩ direction as strain increases. Also, serrated flow and discontinuous slip band propagation were observed.

2. EXPERIMENTAL PROCEDURE

A single crystal was grown from FeAl master ingots by the Bridgman technique. Chemical composition of this crystal is Fe:Al = 61:39 in atomic fraction; in addition, 19 w.p.p.m. Si, 50 w.p.p.m. Cu, and 270 w.p.p.m. C are present as main impurities. After homogenizing at 1373 K for 48 h in vacuum, the single crystal was slowly cooled to room temperature at a rate of 5×10^{-3} K/s.

Rectangular specimens of about $2 \times 2 \times 5$ mm^3 all having the [$\bar{1}$23] compression axis were cut out of the homogenized single crystal by an electro-discharge machine (EDM). All specimen surfaces were ground up to #4000, and then electro-polished.

†Present address: Metals and Ceramics Division, Oak Ridge National Laboratory, P.O. Box 2008, Oak Ridge, TN 37831-6115, U.S.A.

‡To whom all correspondence should be addressed.

Compression tests were conducted in vacuum of better than 10^{-3} Pa at an initial strain rate of about 1.6×10^{-4}/s and temperature of 823 K. (The peak temperature of the yield stress anomaly of this single crystal was found to be about 823 K in our earlier work.) After the compression tests, the specimens were cooled down to room temperature in the furnace. Slip line characteristics on the surfaces were observed with an optical microscope using Nomarski interference contrast, and operative slip planes were determined by the two-surface trace analysis method. Disks were sectioned from the deformed specimens by EDM. Thin foils were made by electropolishing in a Struers Tenupol-3 and a 33% nitric acid–methanol solution at a voltage of 4 V and temperature of 248 K. The thin foils were examined in a Hitachi H-8100D electron microscope at 200 kV.

3. RESULTS

Stress–strain curves of the single crystal at 823 K are shown in Fig. 1. The compression axis is shown in the unit triangle inserted in this figure. As mentioned in the preceding section, the peak temperature of the yield stress anomaly of this specimen lies around this temperature. Interestingly, the deforming crystal exhibited serrated flow within some initial strain (curves *a* and *b*). In this early stage, slip traces show a very inhomogeneous distribution. On the two perpendicular specimen surfaces, as shown in Figs 2(a) and (b), only a few coarse slip bands parallel to the primary slip plane, $(\bar{1}01)$, are observed after the plastic strain of $\varepsilon = 0.5\%$. With increasing strain, the slip bands propagated over the entire length of the specimen like the propagation of Lüders bands. Beyond a certain strain ($\varepsilon \geq 3\%$), serrations disappeared, and instead remarkable work-softening occurred (curve *c*). Two surfaces of the specimen corresponding to curve *c* are shown in Figs 2(c) and (d). Slip bands have already propagated throughout the entire specimen, and slip traces other than the $(\bar{1}01)$ planes are also detected on the surfaces in a small amount. The corresponding slip planes are non-crystallographic ones, slightly deviating from the $(\bar{1}01)$ plane toward the $(\bar{2}11)$ twinning plane for the [111] slip.

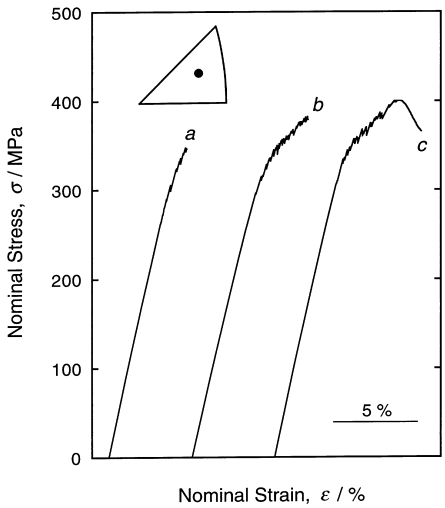

Fig. 1. Nominal stress–strain curves of three specimens deformed at 823 K and to the three different strain levels.

The change of flow behavior, depending on the strains mentioned above, might be associated with a change of dislocation microstructure. To investigate this possibility, deformation microstructures at various strains were observed in transmission electron microscope (TEM). One disk was sectioned from a thick slip band of specimen *a* [Fig. 2(a)], and one thin foil was prepared from it. A few foils parallel to the $(\bar{1}01)$ plane were also obtained from specimens *b* and *c* within their deformed sections.

The dislocation substructure observed in the foil of specimen *a* is shown in Fig. 3. The length of dislocations is relatively short, although the foil was cut almost parallel to the slip bands. And, many dislocation lines are sharply bent. In order to determine the Burgers vector of the dislocations, a typical dislocation substructure was observed under various **g** vectors, as shown in Fig. 4 for instance. Almost all the dislocations are in contrast when $\mathbf{g} = \bar{1}0\bar{1}$ [Fig. 4(b)], whereas, they show some residual contrast when $\mathbf{g} = 1\bar{2}1$ and $01\bar{1}$ [Figs 4(a) and (c)]. This analysis gives that the Burgers vector of those dislocations is parallel to [111]. It should be noted that ⟨111⟩ slip is activated predominantly at the early stage of deformation at the peak temperature. However, the glide decomposition of [111]-type dislocations into [101]- and [010]-type dislocations was not directly observed.

Figure 5 shows two weak-beam micrographs of a dislocation line taken by tilting around the $[1\bar{2}1]$ edge orientation in the foil of specimen *a*. Although the dissociation of the superdislocation could not be discerned in the $[\bar{1}01]$ projection, it can be clearly seen at the portion nearly parallel to the edge orientation, $[1\bar{2}1]$, marked by arrows in the $[\bar{3}\bar{1}1]$ and the $[\bar{1}13]$ projections [Figs 5(a) and (b), respectively]. This evidence shows that this portion is climb-dissociated onto the (111) plane. At the corner of this dislocation configuration, marked by arrows in Fig. 5(a), the superpartial pair can be clearly resolved, but the image of the superpartials is overlapped in Fig. 5(b). This dislocation morphology indicates that the climb-dissociation around this corner occurs on a plane different from the (111) plane. Many ⟨111⟩-type dislocations activated at the early stage of deformation at the peak temperature are climb-dissociated.

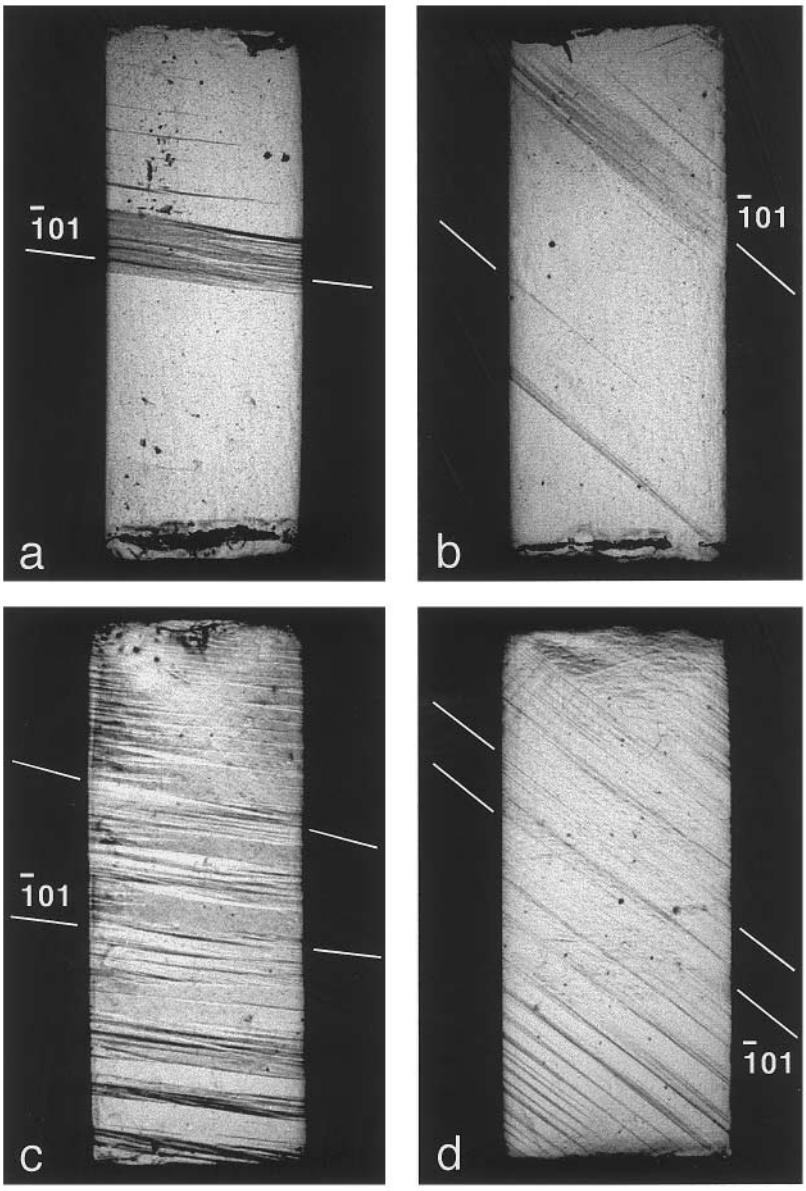

Fig. 2. Slip band observation in optical microscopy: (a) and (b) show two surfaces of the specimen designated as *a*, and (c) and (d) show the specimen designated as *c*.

Figure 6 is a bright-field micrograph showing a dislocation substructure of specimen *b* (Fig. 1), which was strained less than 3% before the strain-softening. Most of the dislocations are out of contrast or in weak residual contrast when $\mathbf{g} = 020$ [Fig. 6(a)], whereas others exhibit a weak, dotted, residual contrast when $\mathbf{g} = 101$ [Fig. 6(b)]. These results of the contrast analysis indicate that the dislocations are of ⟨100⟩-type. We deduce from this evidence that slip direction changes during deformation with increasing strain. However, no evidence of the glide decomposition of ⟨111⟩-type dislocations was found in this microstructure.

4. DISCUSSION

Yoshimi and Hanada [11] observed the decomposed configuration of [111]-type dislocations into [010]- and [101]-type dislocations in the specimen deformed just below the peak temperature. On the basis of this observation, we suggested that the glide decomposition may play a role as a major cause of the strength anomaly in B2 FeAl. Morris *et al.* [2, 13] also observed such a decomposition in polycrystalline iron aluminides strained around the peak temperature. In this work, however, glide decomposition was hardly observed even in the speci-

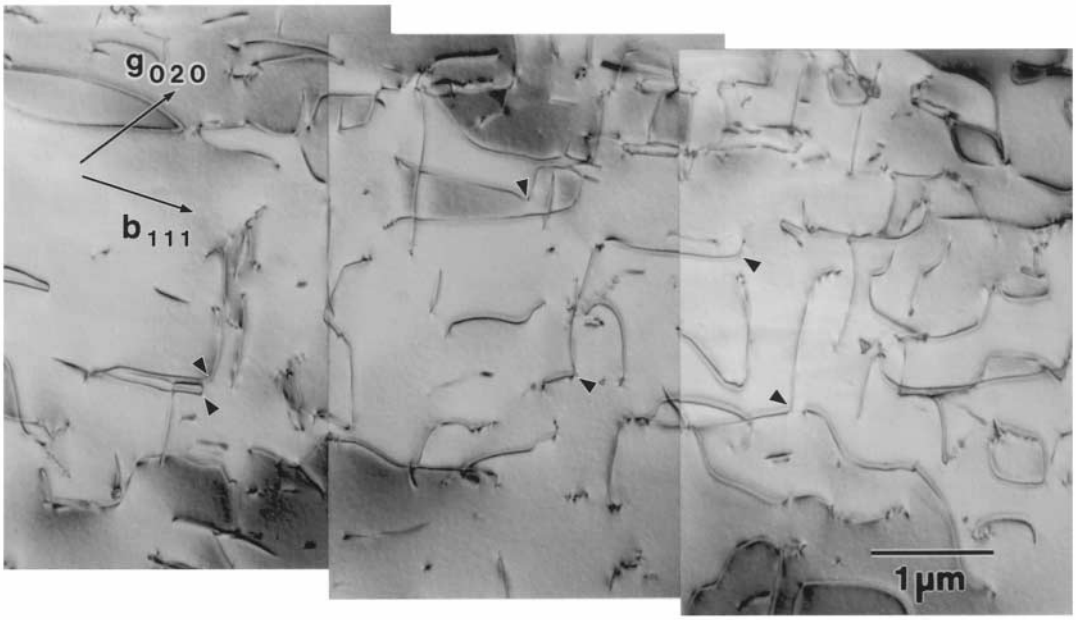

Fig. 3. Bright field electron micrograph taken in specimen *a*. $B \cong [\bar{1}01]$, $\mathbf{g} = 020$.

men deformed at the peak temperature in spite of still significant ⟨111⟩ slip activity. This suggests that such a decomposition may not be a major source for the anomaly. On the other hand, it is found in this work that the slip vector changes from ⟨111⟩ to ⟨100⟩ with increasing strain at the peak temperature. This suggests that the decomposition still occurs during work hardening and it may act as the primary source mechanism for ⟨100⟩-type ordinary dislocations. Indeed, the density of ⟨111⟩-type superdislocations is much lower after the transition ($\varepsilon \approx 3\%$) than before. If the sources of ⟨100⟩-type ordinary dislocations were activated independently of the decomposition, e.g. surface sources, there would have been more ⟨111⟩-type superdislocations left in the sample. In β-CuZn, which has the same B2 structure and the same slip system below the peak temperature as FeAl, slip transition from ⟨111⟩ to ⟨100⟩ directions similar to that observed in our earlier work [11] had been observed in single crystals by Saka and Kawase [14]. Furthermore, they demonstrated that the density of [010] and [101] ordinary dislocations increased while the density of [111] superdislocations decreased around the peak temperature. Their observation also indicates that the glide decomposition may be the main source for ⟨100⟩ ordinary dislocations. As observed in the present work, slip bands propagate inhomogeneously like a Lüders band in single crystal specimens. This means that the amount of plastic strain and work-hardening differs locally from one location to others within a specimen. Although it has not been revealed how the glide decomposition occurs, it is unlikely that the glide decomposition occurs simultaneously over the entire specimen because of its strain-inhomogeneity. This would be the reason why the glide decomposition could not be observed by TEM in the present work.

The work-softening beyond the peak stress shown in curve *c* of Fig. 1 is one of the intrinsic deformation properties of B2 FeAl around the peak temperature. In our earlier work [12], similar behavior was often observed even in the tensile deformation. In addition, after a drastic yield drop, the specimens work-hardened again in the compression deformation [3]. These indicate that the work-softening observed was not caused by any experimental inaccuracy such as a buckling of specimens. Though slightly different orientation, in the similar Fe–39.5Al single crystals under the same strain rate, the amount of stress-drop was obtained by the stress-relaxation experiment to be $\Delta\sigma \approx 30$ [MPa] at 773 K and $\Delta\sigma \approx 120$ [MPa] at 823 K, according to Fig. 3 of Ref. [15]. This indicates that the larger stress-drop around the peak temperature is due to the ⟨111⟩–⟨100⟩ slip transition in association with the work-softening.

To our knowledge, the formation of "slip band bundles" [16] or "Lüders-like slip" [17] has been observed, for the first time, in single crystals of B2-type intermetallic compounds. There are a couple of distinct differences between the present experimental result and other results of single crystals reported in the literature. For instance, under tensile deformation, copper-based alloys [18], 70–30 α-

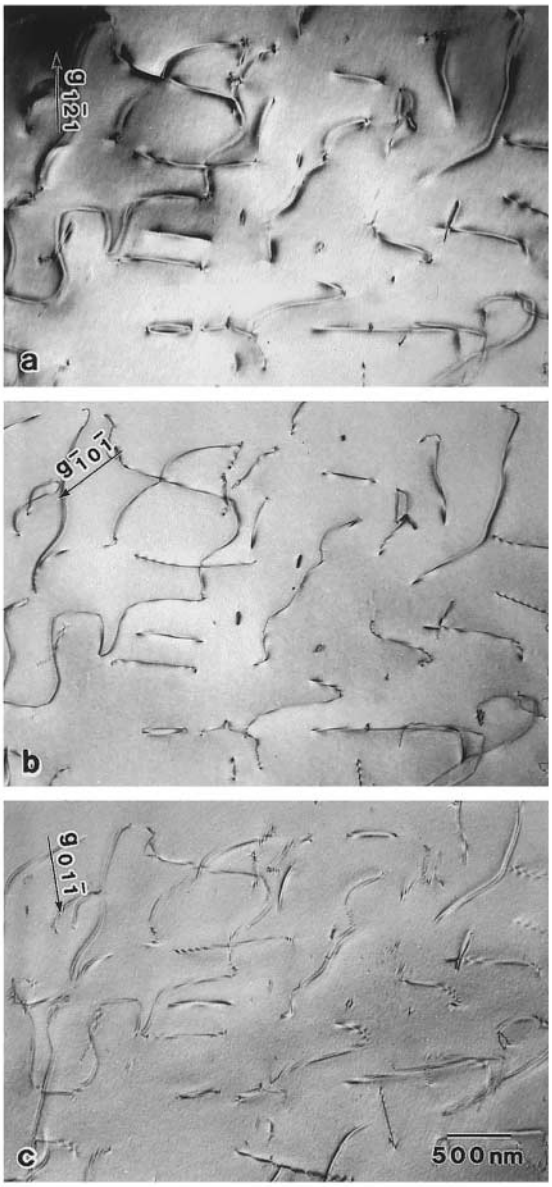

Fig. 4. Bright field electron micrographs taken in the same foil observed in Fig. 3: (a) $B \cong [\bar{1}01]$, $\mathbf{g} = 1\bar{2}1$; (b) $B \cong [\bar{1}01]$, $\mathbf{g} = \bar{1}0\bar{1}$; (c) $B \cong [\bar{1}11]$, $\mathbf{g} = 01\bar{1}$.

brass [19], and nickel-based superalloys [20], all exhibited the yield point and subsequent Lüders band propagation during essentially no work-hardening. Whereas, under compression at 823 K, Fe–39Al single crystals showed the formation of a Lüders-like slip band after the plastic strain of $\varepsilon \approx 0.5\%$ and its propagation throughout the sample up to $\varepsilon \approx 3\%$, exhibiting serrated flow and work-hardening. In addition, the Burgers vector of active dislocations changes from $\langle 111 \rangle$ to $\langle 100 \rangle$ at the end of the Lüders band propagation, beyond which work-softening commences.

A Lüders band is a dislocation avalanche moving into unyielded material, where the coupled dynamics of different dislocation species (if necessary, point defects) is of importance [17]. For β-CuZn alloys, Brindley *et al.* [18] proposed that the model of propagation of coarse slip bands associated with Lüders band extension is related to the extent of dislocation locking by solute atoms. On the other hand, in α-CuZn, the successive, extensive, double cross-slip is believed to play an important role in controlling the slip band propagation [19]. In the present case of Fe–39Al, both mechanisms appear to be involved in the Lüders-like slip band propagation. Optical microscopic observations of slip traces reported earlier [3] indicate ample evidence of cross slip of $[111](\bar{1}01)$ superdislocations onto other planes such as $(\bar{1}10)$ and $(\bar{2}11)$. Since the equilibrium concentration of thermal vacancies in the unyielded part of a sample at 823 K is estimated to be $\approx 1 \times 10^{-4}$ with the vacancy formation energy of 0.98 eV [21], dislocation–vacancy interaction may also play some role in the yield stress anomaly [22] even at this transition temperature.

TEM results of dislocation substructure are consistent with the above interpretations. In Figs 3 and 4, after $\varepsilon = 2.2\%$, dislocation microstructure consists of nearly equal numbers of edge segments and screw dislocations. If all of these dislocation segments were parts of glide loops, i.e. they all lie on the $(\bar{1}01)$ slip plane without any jogs, the angular range of line tension instability with respect to $\mathbf{b} = [111]$ is $\phi = 38$–57° in Fe–40Al at 300 K [23] and $\phi = 37$–60° in Fe–30Al at 1173 K [24]. Some of the sharp corners of the dislocation configuration are consistent with this instability range, e.g. arrows marked in Fig. 3. Many edge and near-edge segments of $\langle 111 \rangle$-type superdislocations are expected to be climb-dissociated at 823 K as shown by Fig. 5, and an increase in number of jogs acquired along the dislocations due to vacancy–dislocation interaction would further influence the dislocation microstructure as shown in Figs 3 and 4.

5. CONCLUSIONS

In this work, slip band propagation and slip vector transition in B2 FeAl were investigated at the peak temperature of the yield stress anomaly. The conclusions are as follows:

1. In single crystals under compression, slip bands resembling Lüders bands propagate, and work-hardening results. The stress–strain curves associated with this behavior are distinctly different from those observed in other single crystalline intermetallics.
2. $\langle 111 \rangle$ slip is activated at the early stage of deformation at the peak temperature. The contribution of glide decomposition of $\langle 111 \rangle$-type

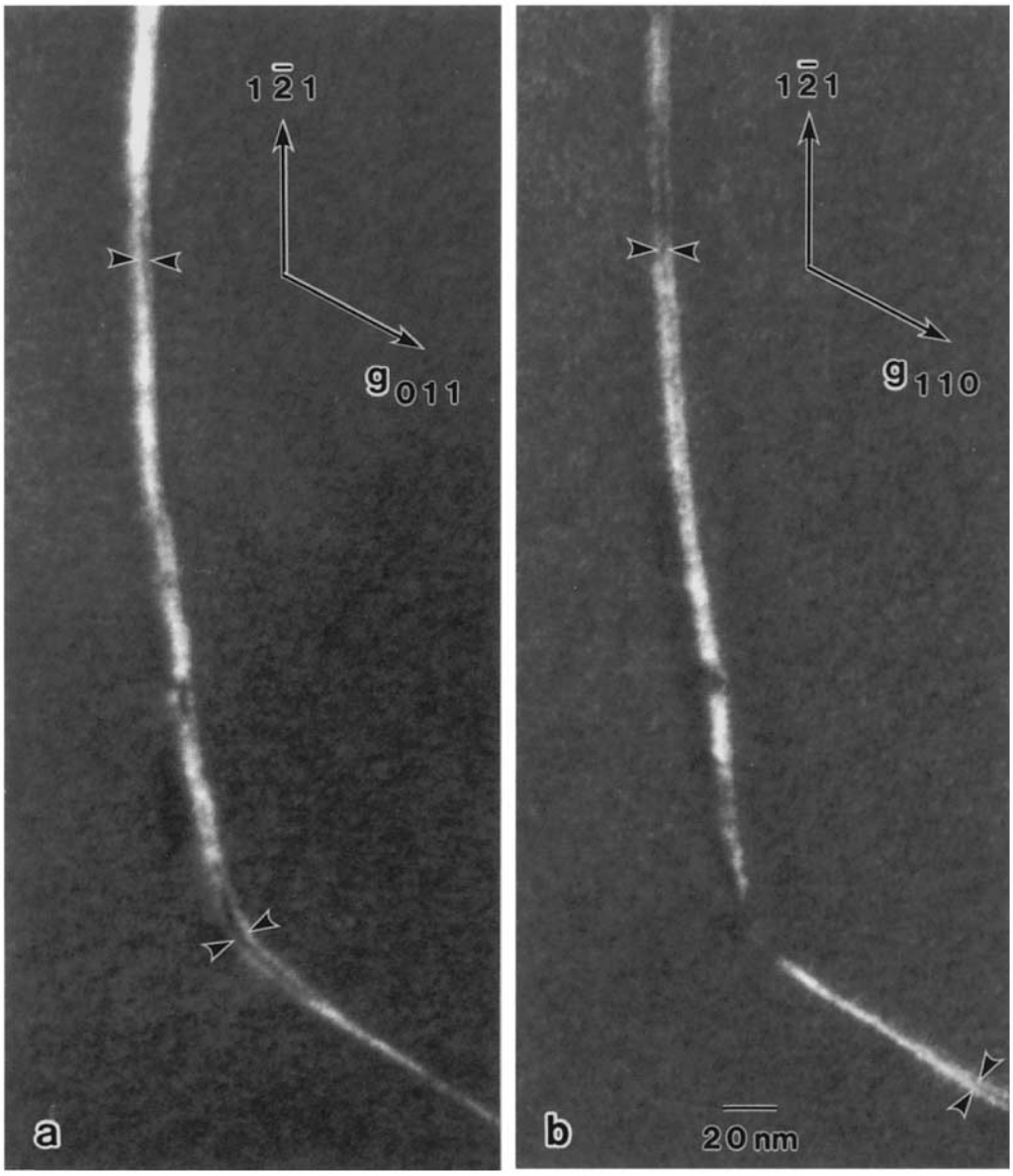

Fig. 5. Weak-beam electron micrographs taken by tilting experiments in the same foil observed in Fig. 3 with **g**–4**g** condition: (a) $B \cong [\bar{3}\bar{1}1]$, **g** = 011; (b) $B \cong [\bar{1}13]$, **g** = 110.

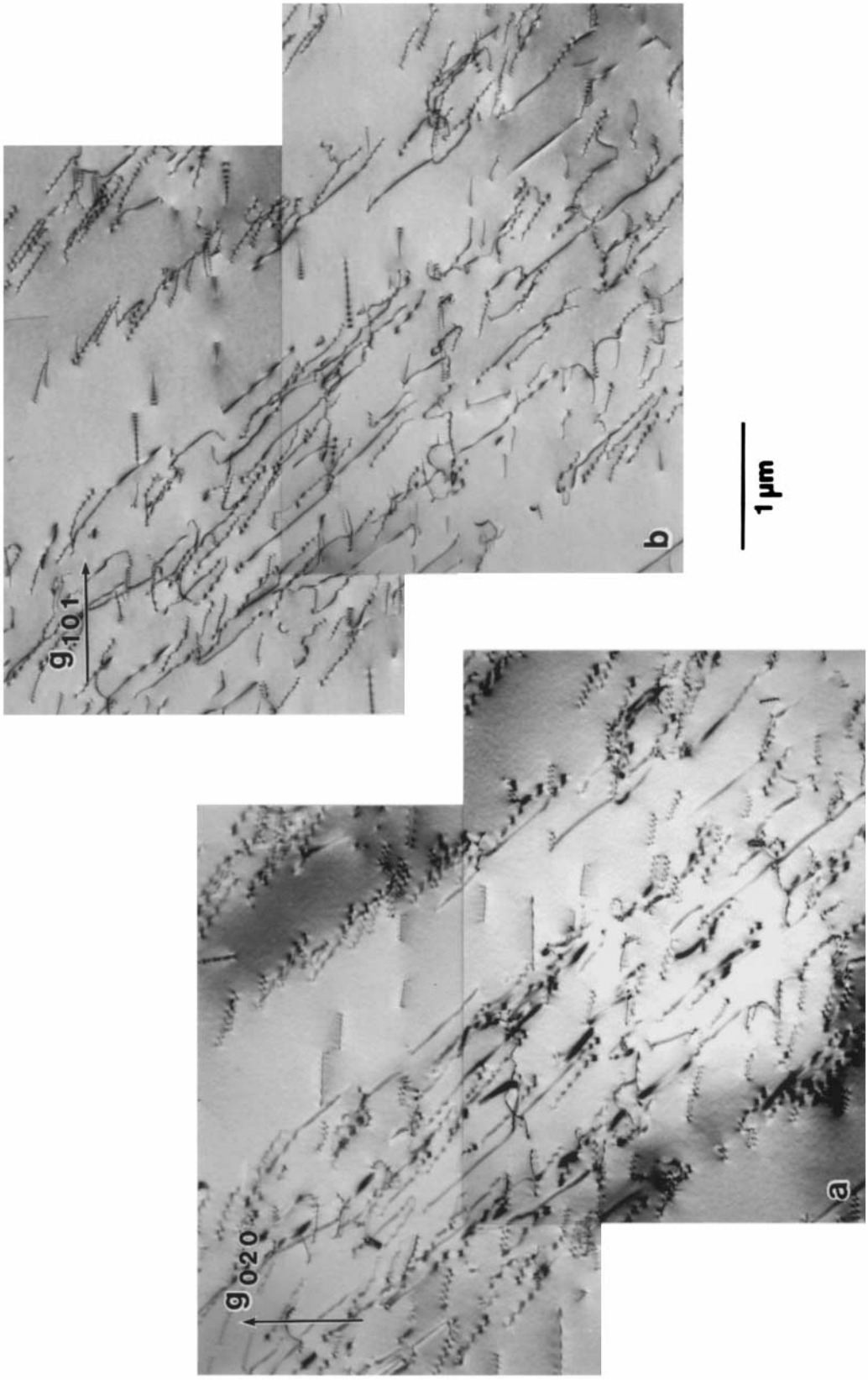

Fig. 6. Bright field electron micrographs taken in the specimen *b*: (a) $\boldsymbol{B} \cong [\bar{1}01]$, $\mathbf{g} = 020$; (b) $\boldsymbol{B} \cong [\bar{1}01]$, $\mathbf{g} = 101$.

dislocations to the yield strength anomaly could not be confirmed.

3. Slip vector changes from ⟨111⟩ to ⟨100⟩ direction with increasing strain. The slip vector that is responsible for the work-softening is ⟨100⟩.

Acknowledgements—The authors thank E. P. George and J. A. Horton for reviewing this paper. This research was sponsored by Grant-in-Aid for Scientific Research on Priority Area from the Ministry of Education, Science and Culture, Japan, and by the Division of Materials Sciences, U.S. Department of Energy, under Contract No. DE-AC05-96OR22464 with Lockheed Martin Energy Research Corp. This research was also supported in part by the program of Japan Society for the Promotion of Science Postdoctoral Fellowships for Research Abroad.

REFERENCES

1. Umakoshi, Y. and Yamaguchi, M., *Phil. Mag. A*, 1980, **41**, 573.
2. Morris, D. G., Peguiron, D. and Nazmy, M., *Phil. Mag. A*, 1995, **71**, 441.
3. Yoshimi, K., Hanada, S. and Yoo, M. H., *Acta metall. mater.*, 1995, **43**, 4141.
4. Mendiratta, M. G., Kim, H. M. and Lipsitt, H. A., *Metall. Trans.*, 1984, **15A**, 395.
5. Matsumoto, N., M.S. thesis, Tohoku University, 1994.
6. Baker, I. and Gaydosh, D. J., *Mater. Sci. Engng*, 1987, **96**, 147.
7. Guo, J., Sun, C., Tan, M., Li, H. and Lai, W., *Acta metall. sin.*, 1990, **3**, 249.
8. Chang, K.-M., *Metall. Trans.*, 1990, **21A**, 3027.
9. Xiao, H. and Baker, I., *Scripta metall. mater.*, 1993, **28**, 1411.
10. Carleton, R., George, E. P. and Zee, R. H., *Intermetallics*, 1995, **3**, 433.
11. Yoshimi, K. and Hanada, S., in *Structural Intermetallics*, ed. R. Darollia, J. J. Lewandowski, C. T. Liu, P. L. Martin, D. B. Miracle and M. V. Nathal. TMS, Warrendale, Pennsylvania, 1993, p. 475.
12. Yoshimi, K., Hanada, S. and Yoo, M. H., *Intermetallics*, 1996, **4**, 159.
13. Morris, D. G. and Morris, M. A., *Intermetallics*, 1997, **5**, 245.
14. Saka, H. and Kawase, M., *Phil. Mag. A*, 1984, **49**, 525.
15. Yoshimi, K., Hanada, S. and Yoo, M. H., in *High Temperature Ordered Intermetallic Alloy VII, MRS Symp. Proc.*, ed. C. C. Koch, C. T. Liu, N. S. Stoloff and A. Wanner, 1996, p. 313.
16. Neuhäuser, H. and Hampel, A., *Scripta metall. mater.*, 1993, **29**, 1151.
17. Hähner, P., *Scripta metall. mater.*, 1993, **29**, 1171.
18. Brindley, B. J., Corderoy, D. J. H. and Honeycombe, R. W. K., *Acta metall.*, 1962, **10**, 1043.
19. Hu, X., Margolin, H., Duan, X. and Nourbakhsh, S., *Scripta metall. mater.*, 1992, **26**, 1257.
20. Kubin, L. P., Lisiecki, B. and Caron, P., *Phil. Mag. A*, 1995, **71**, 991.
21. Würschum, R., Grupp, C. and Schaefer, H.-E., *Phys. Rev. Lett.*, 1995, **75**, 97.
22. George, E. P. and Baker, I., *Phil. Mag. A*, 1998, **77**, 737.
23. Yoshimi, K., Matsumoto, N., Hanada, S. and Yoo, M. H., in *Processing, Properties and Applications of Iron Aluminides*, ed. J. H. Schneibel and M. H. Crimp. TMS, Warrendale, Pennsylvania, 1994, p. 205.
24. Yoo, M. H., Koeppe, M., Hartig, C., Mecking, H., Hermann, W. and Sockel, H.-G., *Acta mater.*, 1997, **45**, 4323.